

This guidance was written prior to the February 27, 1997 implementation of FDA's Good Guidance Practices, GGP's. It does not create or confer rights for or on any person and does not operate to bind FDA or the public. An alternative approach may be used if such approach satisfies the requirements of the applicable statute, regulations, or both. This guidance will be updated in the next revision to include the standard elements of GGP's.

DRAFT OF SUGGESTED INFORMATION FOR REPORTING EXTRACORPOREAL SHOCK
WAVE LITHOTRIPSY DEVICE SHOCK WAVE MEASUREMENTS

FDA requires manufacturers of extracorporeal shock wave lithotripters to characterize the shock waves produced by their devices. In doing so, lithotripter manufacturers should describe the instruments (e.g., hydrophones) and procedures used to measure the shock waves, and present the results of these tests. To assist FDA's review of this information, please use an item numbering scheme that corresponds to the one below, and consecutively number all pages, tables, figures, and equations. Also, please label all figures clearly with captions, axis labels, and units as appropriate.

1. Hydrophone Description and Specifications

1.1. Hydrophone Description

Reference Hydrophones: For faithful reproduction of the shock waveform, including the negative portion of the pulse, the hydrophone should be a piezopolymer (e.g., PVDF) spot-poled membrane type, or a demonstrated equivalent. (It should be noted that some PVDF needle-type hydrophones with acoustically hard backings have not responded well to the trailing negative (rarefactional) portion of some shock waveforms.) One caution in using membrane hydrophones is that their angular response exhibits a sensitivity minimum at an incidence angle of approximately 40 degrees. Thus, errors can result if measurements are made on fields from shock wave sources having sufficiently large apertures.

The hydrophone effective diameter should not exceed 1 mm or $0.2d_6$, whichever is greater, for frequencies greater than 2 MHz. The quantity d_6 is the smallest beam width at which the peak positive (compressional) pressure is down 6 dB (0.5) from its maximum value.

For shock waveforms having rise times greater than 25 ns, the hydrophone membrane thickness should not exceed 50 micrometers. For shock waveforms having rise times less than 25 ns, the hydrophone membrane thickness should not exceed 25 micrometers.

Non-Reference Hydrophones: Because of the wide spectral content and steep rise times associated with lithotripter shock waves, the use of hydrophones whose performance deviates significantly from that of the reference hydrophone is discouraged. Only reference hydrophones are well suited for nearly absolute, accurate characterizing of the pulse shape and beam size of a shock wave field. However, it may be appropriate in some circumstances involving prolonged use to employ hydrophones of lower performance than reference hydrophones, such as in QA or life-testing, or when significant hydrophone damage is unavoidable. For example, the use of non-reference hydrophones may be necessary to produce the plots called for in Section 2 below, especially in 2.2.1.2, 2.2.1.3, and 2.2.1.4.

1.2. Hydrophone Information Requirements

Provide the following information for each type of hydrophone used to make shock wave measurements:

- 1.2.1. end-of-cable sensitivity into specified electrical load vs. frequency (desirable frequency range: 0.2-20 MHz);
- 1.2.2. angular response plot over ± 45 degrees for at least one frequency (recommended frequency: 2 MHz), and calculation of effective diameter, d_e , in mm using $d_e = 0.52c/f\sin\Theta_3$, where c is the speed of sound of the propagation medium in mm/ μ s, f is frequency in MHz, and Θ_3 is the angle at which the angular response is down 3 dB (0.71).

(Effective diameter typically is determined from angular response measurements. There can be an important difference between the physical diameter of the sensor and its effective diameter. Usually the effective diameter is the larger of the two.)
- 1.2.3. a brief description of the measurement techniques used to determine the specifications of 1.2.1. and 1.2.2. (above), if known.
- 1.2.4. overall dimensions;
- 1.2.5. the specifications for any hydrophone amplifier used, including frequency response, maximum output voltage, and, for non-integral amplifiers, the length of cable between the hydrophone and amplifier; (Minimizing this cable length is important in avoiding transmission-line ringing effects.)

- 1.2.6. if the hydrophone(s) is from a commercial source, the manufacturer's name, address, and hydrophone model number.

If a non-reference hydrophone is used to gather any data supplied in the submission, then provide the following information:

- 1.2.7. a list of the data gathered with the non-reference hydrophone;
- 1.2.8. at the maximum shock wave generator output setting, a comparison of the output of the non-reference hydrophone with the output of the reference hydrophone, including the shock waveform at the focus.

2. Measurement Data

Unless stated otherwise below, the following information should be provided for minimum, typical, and maximum shock wave generator output settings and pulse repetition rates.

2.1. Temporal Information

The description of the temporal characteristics of the shock wave pulse should include a time domain representation of the shock waveform at the focal maximum (i.e., the point where the peak positive pressure is a maximum), as measured by a reference hydrophone. Note that the position of the focal maximum may vary as the shock wave generator output setting is changed (see 2.2.3).

Using the waveform from above, provide the following:

- 2.1.1. a frequency domain representation of the shock waveform;
- 2.1.2. the peak positive and peak negative pressures of the shock waveform, in units of pascals (MPa, kPa, etc.);
- 2.1.3. the rise time and pulse width of the shock waveform, where pulse width is defined as the time between the half amplitude points on the initial positive pressure half cycle;
- 2.1.4. the peak positive pressure vs shock wave generator output setting, over the full range of output settings available to the user.

2.2. Spatial Information

Assuming x-y-z coordinates, with the z-direction being axial and the x- and y-axes being lateral, provide the following information about the spatial characteristics of the shock wave field:

(Note: For the purposes of this Section, a beam is symmetric if the smallest and largest lateral positive pressure beam widths differ from their mean value by no more than 10%.)

2.2.1. two-dimensional and contour plots for peak pressures around the focus as follows:

2.2.1.1. 2-D lateral beam plots of peak positive and peak negative pressures along x- and y-axes at the focus;

2.2.1.2. 2-D axial beam plot of peak positive pressure along the z-axis;

2.2.1.3. if the beam is symmetric, contour (isobar) plots of peak positive pressure at a typical shock wave generator output setting in x-z OR y-z plane;

2.2.1.4. if the beam is not symmetric, contour (isobar) plots of peak positive pressure at a typical shock wave generator output setting in x-z AND y-z planes; (Here x- and y-directions correspond to minimum and maximum beam widths, which are assumed to be located along perpendicular axes. Please indicate if this is not the case.)

2.2.1.5. spatial sampling increments (dx, dy, dz), and justification for their choice;

2.2.2. a description of the focal region in terms of the -6 dB beam widths, for peak positive pressure along the x-, y-, and z-axes, and for peak negative pressure along the x- and y-axes.

2.2.3. a description of any variation in peak positive pressure location (from 2.2.1.2) and -6 dB beam widths (2.2.2) as a function of the shock wave generator output setting.

2.3. Beam Energy

Provide a calculation of the energy per pulse by integrating the field over the -6 dB beam surface at the focal maximum.

The energy in a lithotripsy pulse at the focus can be approximated by the expression,

$$E = Z^{-1} \int \int_S p^2(r, \Theta, t) dt dS, \quad (1)$$

where r and Θ are spatial polar coordinates over the focal surface S , t is time, p is the acoustic pressure function, and Z is the acoustic impedance of water, nominally 1.5×10^6 mks units (rayls). For a beam with circular symmetry,

$$E = 2\pi \int_0^R PII(r) r dr, \quad (2)$$

where $PII(r)$, the pulse intensity integral at lateral distance r , is

$$PII(r) = Z^{-1} \int p^2(r, t) dt. \quad (3)$$

For the purposes of this calculation, R in equation (2) is the -6 dB beam radius based on a plot of the peak positive pressure. In evaluating E , the results of four radii along two orthogonal diameters should be averaged. One numerical solution of equation (2) is

$$E = 0.5\pi \sum_{i=1}^N (PII_i + PII_{i-1})(R_i^2 - R_{i-1}^2). \quad (4)$$

Here it is assumed that a measurement of the beam has been made laterally at $N+1$ points between $r=0$ and $r=R$, and that the pulse intensity integral at point $r=R_i$ is PII_i . Also, $R_0=0$ and $R_N=R$.

3. Measurement Techniques

Provide details of the measurement technique, including:

- 3.1. the placement scheme of the shock wave source and hydrophone used to determine the information gathered in number 2 (above) (e.g. hydrophone mounting, positioning, and alignment relative to source);
- 3.2. the analog bandwidth, sampling rate, and number of bits of the digitizer employed; (For accurate measurement of rise time, t_r , the sampling rate should be greater than approximately $5/t_r$.)
- 3.3. an assessment of the systematic and random errors involved in making these measurements, including a brief

description of all relevant errors considered and an explanation of how the overall error was determined.

- 3.3.1. an assessment of the effects of shock-to-shock variability on measurement accuracy, including variations in the pulse quantities in 2.1.2 and 2.1.3, and beam widths in 2.2.2.

LITHOTRIPSY PULSE MEASUREMENT ERRORS DUE TO NON-IDEAL
HYDROPHONE AND AMPLIFIER FREQUENCY RESPONSE

Gerald R. Harris

Center for Devices and Radiological Health
Food and Drug Administration
5600 Fishers Lane, HFZ-132, Rockville, MD 20857

Abstract - When using miniature ultrasonic hydrophones to probe the focal region of extracorporeal shock wave lithotripsy devices, the frequency response of the measurement hydrophone and any associated amplifier must be broad enough to minimize pulse distortion. To study the potential effects of bandwidth-limited behavior on lithotripsy pulse measurements, a mathematical model used previously for diagnostic-type pulses was modified [G.R. Harris, 1989 IEEE Ultrasonics Symposium Proceedings, pp. 1061-1065]. Several parameters of a simulated lithotripsy pulse were compared before and after being filtered by hydrophone and amplifier response functions, both separately and in combination. Errors were computed for the peak positive and negative pressures, rise time, pulse duration, and pulse intensity integral as functions of hydrophone and amplifier bandwidths. Although most of the energy in a shock wave pulse lies at frequencies below a few megahertz, significant errors can occur unless measurement bandwidths are much wider. For example, for a 20 ns rise-time pulse, the bandwidths of the hydrophone or amplifier acting separately should extend beyond 40-50 MHz to keep rise time errors below 10%. However, because the two response functions can compensate one another to some extent, accuracy for the combined response can be maintained at lower bandwidths if the amplifier's cut-off frequency is less than the hydrophone's thickness resonance peak.

I. INTRODUCTION

At the focus of an extracorporeal shock wave lithotripsy (ESWL) device's shock wave field, pressure pulses are characterized by an initial compressional (positive) half cycle having a rapidly rising leading edge, followed by a more slowly varying rarefactional (negative) half cycle [1]. After the negative pressure peak, the pressure amplitude gradually decreases, either monotonically or with damped oscillations. Because this slowly varying pressure "tail" can persist for many microseconds, most of the energy in an ESWL pulse lies at frequencies below a few megahertz. However, at the highest ESWL generator settings, positive pressure rise times typically are less than 50 ns, and may be less than 10 ns. Therefore, a wide bandwidth hydrophone and amplifier are necessary to reproduce faithfully all the features of the ESWL pulse.

Coleman and Saunders have made useful experimental comparisons of the responses of different hydrophones to a shock wave pulse [2]. However, their study did not include a quantitative

analysis of the errors associated with these measurements. In a previous paper by this author the effects of hydrophone and amplifier frequency response on the measurement of diagnostic ultrasound pulses were studied theoretically [3]. In this paper a similar approach is applied to pulses typical of those encountered in ESWL devices. After describing the theoretical model in Section II, various simulation results are presented in Section III. Also considered in Sec. III are the effects of undersampling by the waveform recording device. Section IV concludes with suggested rules of thumb for choosing hydrophone and amplifier bandwidths.

II. DESCRIPTION OF MODEL

Figure 1 contains a block diagram of the pulse response model. The pressure $p_i(t)$ represents the ESWL pulse as a function of time, t ; $p_o(t)$ is the pulse after being filtered by the hydrophone and amplifier response functions, $H_h(f)$ and $H_a(f)$, respectively, f being frequency. Thus, $p_o(t)$ is found from

$$p_o(t) = F^{-1}\{P_i(f) \cdot H_h(f) \cdot H_a(f)\}, \quad (1)$$

where $P_i(f)$ is the Fourier transform of $p_i(t)$, and F^{-1} denotes an inverse Fourier transform. The mathematical forms of $p_i(t)$, $H_h(f)$, and $H_a(f)$ are discussed below.

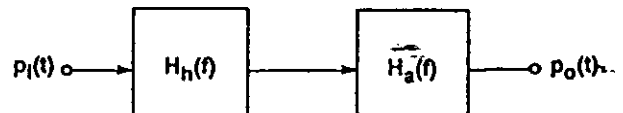


Figure 1 - Block diagram of pulse response model.

A. ESWL Pressure Pulse

The general form for $p_i(t)$ used in this study was similar to that described by Church [4]. It comprises the product of falling and rising exponentials and a sinusoid, as in Eq. (2).

$$p_i(t) = e^{-\alpha t} (1 - e^{-\beta t}) \sin[2\pi f(t_1 - t)] \quad (2)$$

Gerald Harris

Although it is difficult to define a typical pulse shape, proper choices of the constants α , β , f , and t_1 in Eq. (2) can give pulses that closely mimic those observed experimentally using the best available measurement techniques [1]. These constants were adjusted to achieve desired values for the rise time (t_r), pulse width (t_w , defined as the time between the half amplitude points on the initial positive pressure half cycle), and peak positive to negative pressure ratio (p_c/p_r). For example, with $\alpha = 1 \mu s^{-1}$, $\beta = 86 \mu s^{-1}$, $f = 0.1$ MHz, and $t_1 = 1 \mu s$, the pulse in Fig. 2 results. This pulse has a rise time of 20 ns, a pulse width of 370 ns, and a p_c/p_r ratio of 6.6.

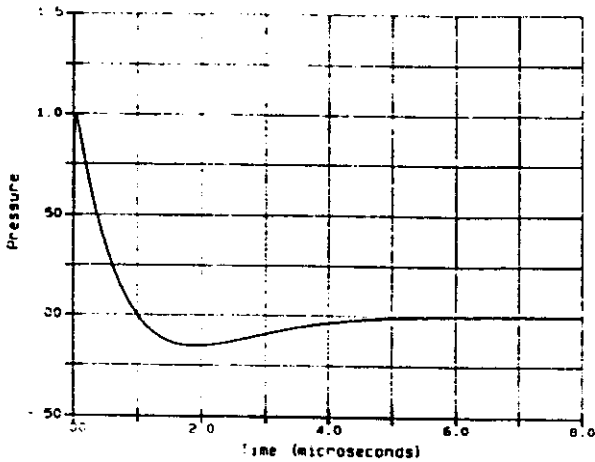


Figure 2 - Simulated ESWL pulse $p_i(t)$. See Pulse #2 in Table I.

Table I contains data on this pulse and five others used in the simulations. Rise times range from 10 ns to 80 ns. Pulse widths are between 300 ns and 400 ns, except for Pulse #5, for which $t_w = 200$ ns. Pressure ratios vary from approximately four to eight.

TABLE I

Values for constants in Eq. (2) expression for $p_i(t)$, and calculated rise times, pulse widths, and positive/negative pressure ratios

Pulse #	α (μs^{-1})	β (μs^{-1})	f (MHz)	t_1 (μs)	t_r (ns)	t_w (ns)	p_c/p_r
1	1	190	0.1	1.0	10	350	6.9
2	1	86	0.1	1.0	20	370	6.6
3	1.5	96	0.5	0.6	20	330	4.2
4	1.05	37.5	0.1	1.0	40	390	6.5
5	3.8	27	0.7	0.4	40	200	8.2
6	1.8	14	0.5	0.6	80	340	4.1

Values of $p_i(t)$ were computed at 4096 equally-spaced points over an 8 μs interval, giving an equivalent sampling increment of 1.95 ns. All Fast Fourier Transform computations were done on 4096-point arrays.

B. Amplifier and Hydrophone Responses

The hydrophone's amplifier response, $H(f)$, was modeled as a single-pole, low-pass filter with low-pass (-3 dB) corner frequency, f_c (see [3], Eq. (2)). The hydrophone response, $H_h(f)$, was derived using Mason's model for a symmetrically loaded piezoelectric receiver [5]. The hydrophone's thickness resonance frequency is denoted by f_n (see [3], Eq. (4)).

C. Pressure Pulse Calculations

Five quantities were calculated on the pulse before and after filtering; that is, on $p_i(t)$ and $p_o(t)$. They were peak positive pressure (p_p), peak negative pressure (p_r), pulse pressure-squared integral (p^2I), rise time, and pulse width. Pulse width and rise time were computed via linear interpolation between sample points. An error value, defined as the percent deviation of $p_o(t)$ from $p_i(t)$, was computed for each of these five quantities.

III. SIMULATION RESULTS

A. Amplifier Response

First the effect of the amplifier acting alone on $p_i(t)$ was considered for 50 values of f_c from 2 MHz to 100 MHz. The error for the five pulse quantities all approached zero monotonically with increasing frequency. The errors for p_p , p_r , and p^2I were negative (i.e., the $p_o(t)$ quantities were smaller); those for t_r and t_w were positive.

As an example, Table II contains frequencies at which the error for the five quantities fall below +5% and +10% for the Pulse in Fig. 2. One can see that, except for rise time, a bandwidth of approximately 10 MHz will result in deviations of +5% or less. Also, for a given f_c , p_r and p^2I can be measured more accurately than the other quantities because of their relatively small high frequency content.

TABLE II

Values of f_c (MHz) at which errors are less than +5% and +10% for Pulse #2 in Table I

Error	p_c	p_r	p^2I	t_r	t_w
< +5%	9	1	5	69	11
< +10%	5	<1	3	46	7

For a pulse $p_i(t)$ almost identical to the one in Fig. 2, but with $t_r = 10$ ns (Table I, Pulse #1), values of $f_c = 18$ and 10 MHz result in errors

Gerald Harris

below $\pm 5\%$ and $\pm 10\%$, respectively, except for rise time. For the error in t_r to be less than or equal to $\pm 5\%$, f_h must be greater than 100 MHz; for $\pm 10\%$, $f_h \geq 94$ MHz.

B. Hydrophone Response

The variation in error with frequency was more variable for the hydrophone response. The

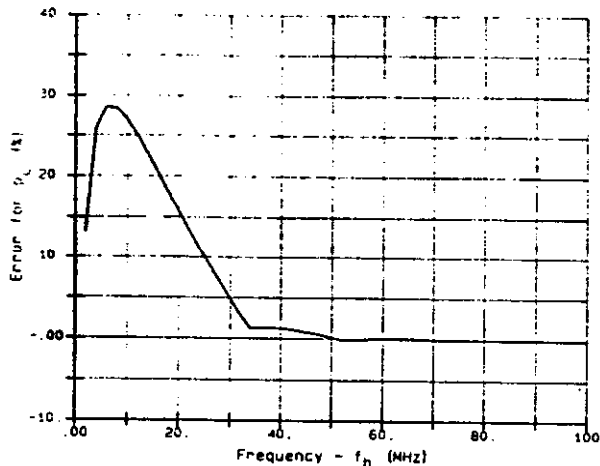


Figure 3 - Error for peak positive pressure (p_c) as a function of hydrophone resonance frequency (f_h) for the pulse in Fig. 2.

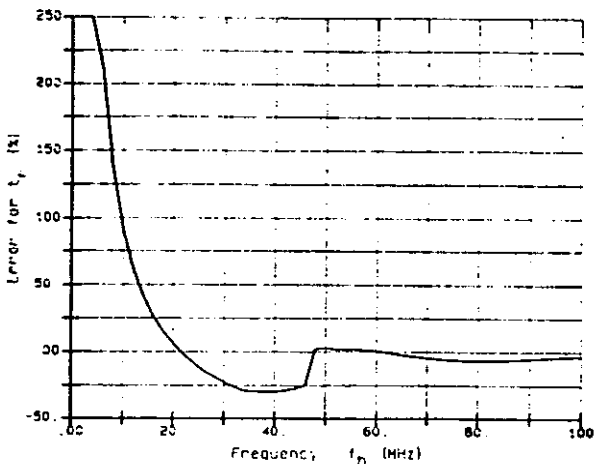


Figure 4 - Error for rise time (t_r) as a function of hydrophone resonance frequency (f_h) for the pulse in Fig. 2. Errors greater than 250% are not plotted.

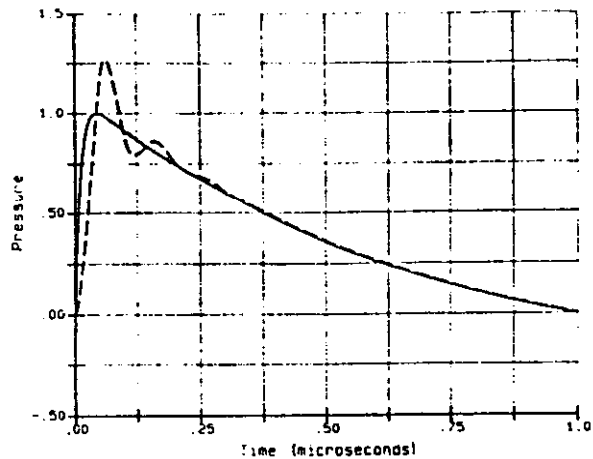


Figure 5 - $p_i(t)$ (solid) and $p_o(t)$ (dashed) for hydrophone response to Fig. 2 pulse with $f_h = 10$ MHz.

difference is due to the thickness resonance peak in $H_h(f)$, a trait common to hydrophones of the spot-poled membrane type [6, 7]. To illustrate, Figs. 3 and 4 contain plots of the error for p_c and t_r as a function of f_h for the pulse in Fig. 2. In Fig. 3 the error for p_c reaches a positive peak at about 5 MHz, falls rapidly to less than 2% at 34 MHz, and remains close to zero thereafter. The error for t_r in Fig. 4, although initially positive and quite large, passes through 0% just above 20 MHz, reaches a negative peak of about -30% at 35-40 MHz, then rises quickly to cross the axis again at approximately 50 MHz, after which the change is relatively small. There is a negative error peak of about -5% at $f_h = 80$ MHz.

The changes in both of these plots are due to the oscillations induced in $p_o(t)$ by the hydrophone's resonance peak. As an example, Fig. 5 contains the first microsecond of $p_i(t)$ and $p_o(t)$ for $f_h = 10$ MHz. Prominent are the first two oscillatory peaks at approximately 70 ns and 160 ns (cf. [2], Fig. 3). As f_h 's increased the amplitude of the first peak decreases with respect to the second, and the two become equal at $f_h = 34$ MHz, the breakpoint in Fig. 3. Between 45 and 50 MHz the first peak falls below 90% of the second, which accounts for the rapid increase in the rise time of $p_o(t)$ just below 50 MHz in Fig. 4. (Recall that rise time is related to the 10% and 90% amplitude points on $p_i(t)$ or $p_o(t)$.)

Table III gives $\pm 5\%$ and $\pm 10\%$ error values for f_h analogous to Table II. A bandwidth greater than about 50 MHz would keep errors less than 5% for the pulse in Fig. 2. For the 10 ns rise time pulse, the error plots corresponding to Figs. 3 and 4 have similar shapes, but all the features described above occur at approximately twice the f_h values. Likewise, the f_h values in Table III approximately double for p_c , t_r , and t_v .

Gerald Harris

TABLE III

Values of f_h (MHz) at which errors are less than $\pm 5\%$ and $\pm 10\%$ for Pulse #2 in Table I

Error	p_c	p_r	p^2I	t_r	t_w
$< \pm 5\%$	30	1	5	48	31
$< \pm 10\%$	25	1	2	47	27

C. Combined Response

To study the effects of the combined amplifier and hydrophone response, f_a was varied from 2 MHz to 100 MHz in steps of 2 MHz, for f_h values of 20, 40, and 80 MHz. These three f_h values correspond to membrane hydrophone film thicknesses of approximately 50, 25, and 12 μm , respectively.

Plots of the error vs f_a in response to the Fig. 2 pulse are given in Fig. 6a-d for p_c , p^2I , t_r , and t_w . Unlike the equivalent plots for $H_h(f)$ in Figs. 3 and 4 above, here all traces are single-valued. Also, the final values (i.e., the $f_a = 100$ MHz values) are not necessarily the

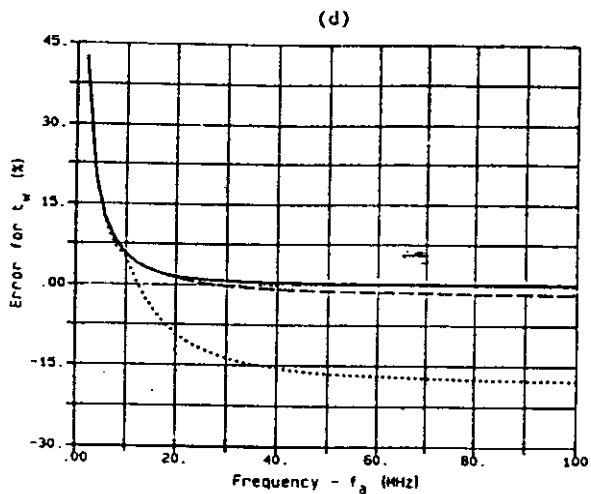
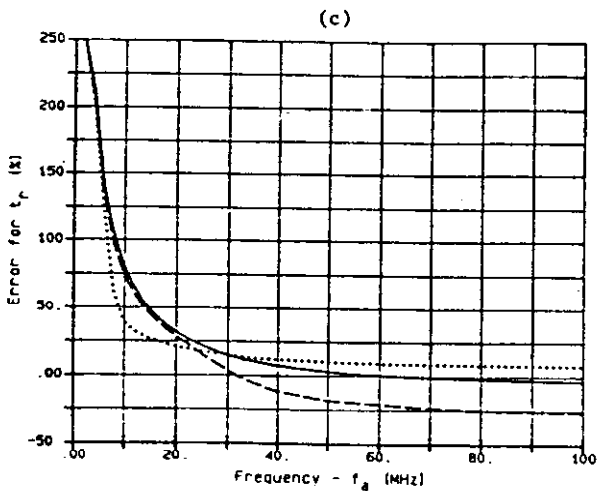
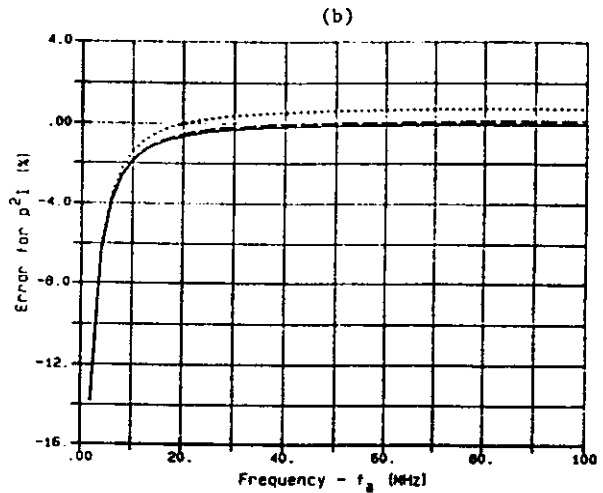
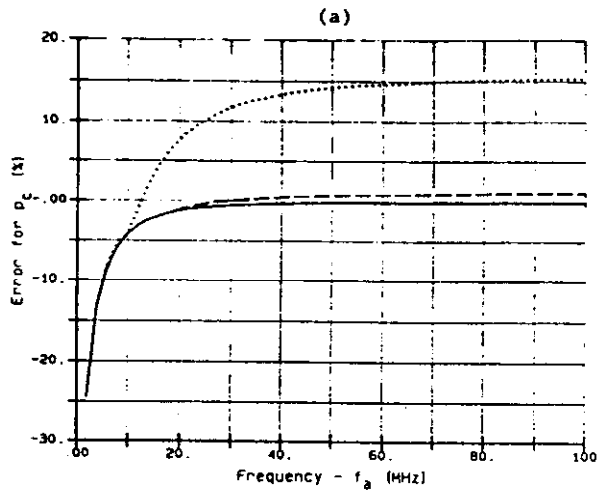


Figure 6 - Error vs f_a for combined hydrophone/amplifier response to Fig. 2 pulse at $f_h = 20$ MHz (dotted), $f_h = 40$ MHz (dashed), and $f_h = 80$ MHz (solid). (a) p_c ; (b) p^2I ; (c) t_r ; (d) t_w . In (c), errors greater than 250% are not plotted.

Gerald Harris

lowest values, because most of the curves cross 0% at a value of f_s less than or approximately equal to f_h . Furthermore, for the case of rise time in Fig. 6c, the $f_s = 100$ MHz value for $f_h = 20$ MHz is less than the value for $f_h = 40$ MHz; that is, the hydrophone with the smaller bandwidth seems to be more accurate. Though not an intuitive result, it is consistent with Fig. 4, which can be considered an error plot for t_r vs f at $f_h = \infty$. (Compare the errors at 20 MHz and 40 MHz in Fig. 4.)

Figure 7 contains the first microsecond of $p_s(t)$ and $p_o(t)$ for $f_s = 30$ MHz and $f_h = 40$ MHz, where $p_i(t)$ is the pulse in Fig. 2. In this case the error for t_r is approximately 3%, and the other errors are all within +1%. For the 10 ns rise time pulse, $f_s = 60$ MHz and $f_h = 80$ MHz give similar results.

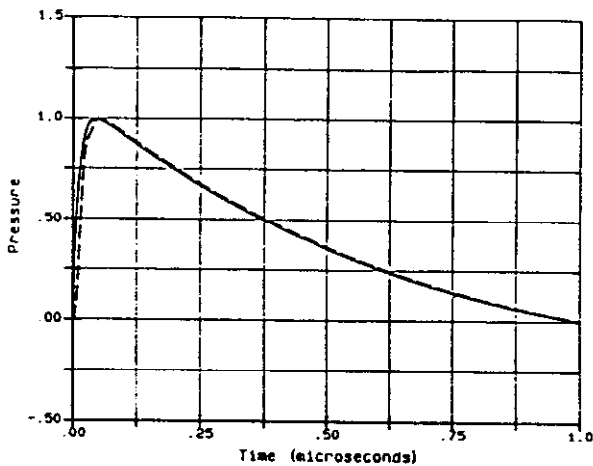


Figure 7 - $p_i(t)$ (solid) and $p_o(t)$ (dashed) for combined hydrophone/amplifier response to Fig. 2 pulse with $f_s = 30$ MHz and $f_h = 40$ MHz.

The error for p_o was not plotted in Fig. 6 because, for values of f greater than 1-2 MHz, the error was less than 5%. The only situation studied in which the error for p_o exceeded 5% at $f_s = 2$ MHz was when f in Eq. (2) was increased, as could be encountered with piezoelectric lithotripters [1]. For example, using Pulse #3 in Table I, which has a frequency f of 500 kHz (Fig. 8), the error for p_o was between 5% and 10% at $f_s = 2$ MHz. In no case considered in Table I was the error for p_o significantly greater than 10% until f_s fell below 2 MHz.

D. Errors Induced by Undersampling

With a sampling increment of 1.95 ns (Sec. II.A), the sampling rate for the various ESWL pulses modeled was approximately 500 MHz. To examine what effect decreasing this rate could have on pulse measurements, rise time and peak positive pressure values for sampling rates at 50, 100, and 250 MHz were compared to the "true" values at 500 MHz. Maximum rise time errors for 10 ns and

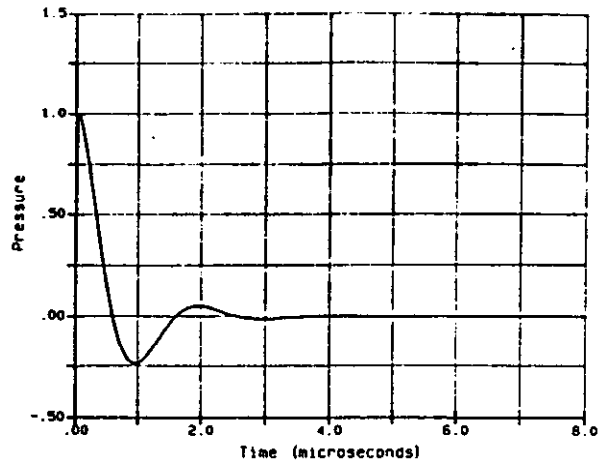


Figure 8 - Simulated ESWL pulse $p_i(t)$. See Pulse #3 in Table I.

20 ns rise time pulses (Pulses #1 and #2 in Table I) are given in Table IV.

As can be seen from Table IV, rise time measurements can be affected significantly by undersampling the time waveform. As a rule of thumb, the sampling interval should be at least five times smaller than the measured rise time.

TABLE IV

Maximum rise time errors due to undersampling for pulses with $t_r = 10$ ns and 20 ns

Sampling Rate (MHz)	$t_r = 10$ -ns	Error $t_r = 20$ ns
50	210%	62%
100	62%	22%
250	15%	4.0%

Corresponding errors for p_o were quite small, exceeding 1% only at 50 MHz for the 10 ns rise time pulse. This small error is due to the fact that the fall time for the initial positive pressure half cycle is much larger than the rise time, typically being hundreds of nanoseconds in duration.

IV. CONCLUSIONS

The usefulness of the analysis in this paper is dependent on how well the functional forms of $p_i(t)$, $H(f)$, and $H_s(f)$ match real world situations. With regard to $p_i(t)$, Figs. 2 and 8, as well as the other pulses represented in Table I, are similar to experimentally observed pulses.

Gerald Harris

In practice ESWL pulses having rise times less than the 10 ns lower limit considered here are conceivable, but accurate measurements below 10 ns are beyond the capabilities of current technology. Furthermore, it is not clear how much such refined knowledge would add to safety or effectiveness studies of ESWL devices.

With regard to the hydrophone and amplifier response models, the $H_a(f)$ used is applicable primarily to membrane type piezopolymer hydrophones. However, at least one needle type hydrophone that has been used to measure ESWL pulses displays no resonance peak, and begins rolling off at about 10 MHz [8]. If the frequency response of this hydrophone is approximated by the amplifier response $H_a(f)$ with $f_a = 10$ MHz, then the results in Sec. III.A can be used to estimate its performance. (Note that in [2], at least one of these needle probes has been found to have diminished low frequency response, a feature not examined here.)

Based on simulations of the pulses in Table I, the two rules of thumb below can be used to assist in choosing hydrophone and amplifier bandwidths, given an expected value for the rise time.

- 1) Bandwidths equal to or greater than $1/t$ will keep rise time errors less than about 10%, and other pulse quantity errors less than about 2%.
- 2) Bandwidths equal to or greater than $1/2t$ will keep rise time errors less than about 30%, and other pulse quantity errors less than about 15%.

In Sec. III.C an example was given of how accuracy for the combined hydrophone/amplifier response could be maintained at lower bandwidths by choosing an f_a a little less than f_b (In the example, $f_a = 0.75f_b$). However, optimal selection of f_a and f_b requires some a priori knowledge of the pulse to be measured.

In addition to these bandwidth considerations, the sampling rate of any waveform digitizer used should be greater than approximately $5/t_r$ to keep rise time errors due to undersampling small (less than a few percent).

REFERENCES

[1] A.J. Coleman and J.E. Saunders, "A survey of the acoustic output of commercial extracorporeal shock wave lithotripters," *Ultrasound in Med. & Biol.*, vol. 15, no. 3, pp. 213-227, 1989.

[2] A.J. Coleman and J.E. Saunders, "A comparison of PVDF hydrophone measurements in the acoustic field of a shock wave source," in *Extra- und Intrakorporale Lithotripsie bei Harn-, Gallen-, Pankreas- und Speichelsteinen*, Ch. Ell, M. Marberger, and P. Berlien, eds. (Georg Thieme Verlag Stuttgart, New York, 1990) pp. 14-22 (in English).

[3] G.R. Harris, "A model of the effects of hydrophone and amplifier frequency response on ultrasound exposure measurements," *Proc. 1989 Ultrasonics Symposium (IEEE, New York, 1989)*, pp. 1061-1065.

[4] C.C. Church, "A theoretical study of cavitation generated by an extracorporeal shock wave lithotripter," *J. Acoust. Soc. Am.*, vol. 86, no. 1, pp. 215-227, 1989.

[5] W.P. Mason, *Electromechanical Transducers and Wave Filters*, (Von Nostrand, Princeton, 1948) 2nd ed.

[6] D.R. Bacon, "Characteristics of a pvdf membrane hydrophone for use in the range 1-100 MHz," *IEEE Trans. Sonics Ultrason.*, vol. SU-29, no. 1, pp. 18-25, 1982.

[7] G.R. Harris, "Hydrophone measurements in diagnostic ultrasound fields," *IEEE Trans. Ultrason. Ferroelec. Freq. Contr.*, vol. 35, no. 2, pp. 87-101, 1988.

[8] M. Platte, "A polyvinylidene fluoride needle hydrophone for ultrasonic applications," *Ultrasonics*, vol. 23, no. 3, pp. 113-118, 1985.